

Chapter 5

The Quasicontinuum Method: Theory and Applications

Dennis M. Kochmann and Jeffrey S. Amelang

5.1 Introduction

The state of the art in material modeling offers highly accurate methods for each individual scale, from density functional theory (DFT) and molecular dynamics (MD) at the lower scales all the way up to continuum theories and associated computational tools for the macroscale and structural applications. Unfortunately, a wide gap exists due to a lack of models applicable at the intermediate scales (sometimes referred to as *mesoscales*). Here, the continuum hypothesis fails because the discreteness of the atomic crystal becomes apparent, e.g., through the emergence of size effects. At the same time, atomistic techniques tend to incur prohibitively high computational expenses when reaching the scales of hundreds of nanometers or microns. Mastering this gap between atomistics and the continuum is the key to understanding a long list of diverse open problems. These include the mechanical response of nanoporous or nanostructured (i.e., nanocrystalline or nanotwinned) metals, the effective mechanical properties of nanometer- and micron-sized structures, devices and engineered (meta)materials, further the underlying mechanisms leading to inelasticity and material failure, or heat and mass transfer in nanoscale materials systems. Overall, there is urgent need for techniques that bridge across length and time scales in order to accurately describe, to thoroughly understand, and to reliably predict the mechanics and physics of solids (Fig. 5.1).

D.M. Kochmann (✉)
California Institute of Technology, Graduate Aerospace Laboratories, 1200 E California Blvd
MC 105-50, Pasadena, CA 91125, USA
e-mail: kochmann@caltech.edu

J.S. Amelang
Harvey Mudd College, 301 Platt Blvd, Claremont, CA 91711, USA
e-mail: jamelang@caltech.edu

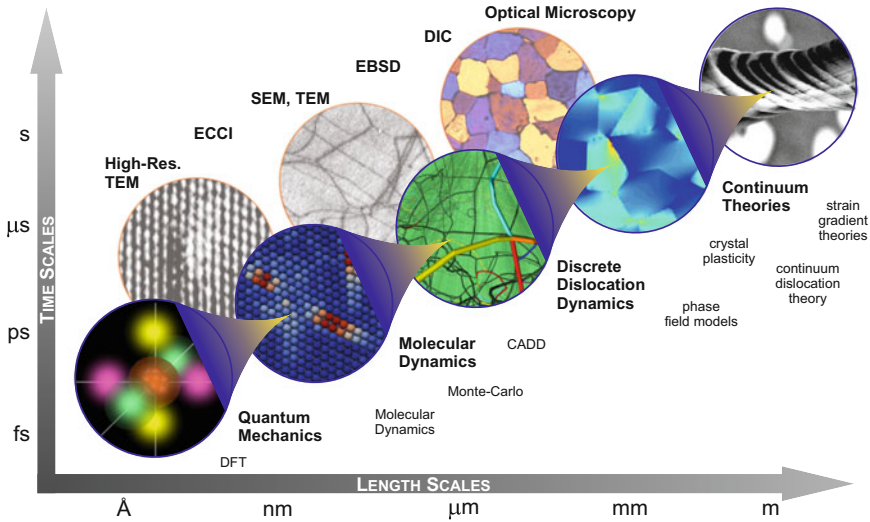


Fig. 5.1 Bridging across scales in crystalline solids: from the electronic structure all the way up to the macroscale (including some of the prominent modeling and experimental techniques). Abbreviations stand for Coupled Atomistic/Discrete-Dislocation (CADD), Density Functional Theory (DFT), Digital Image Correlation (DIC), Electron Back-Scatter Diffraction (EBSD), Electron Channelling Contrast Imaging (ECCI), and Scanning/Transmission Electron Microscopy (SEM/TEM)

Over the decades, various methodologies have been developed to bridge across scales. On the one hand, *hierarchical* schemes are the method of choice when a clear separation of scales can be assumed. In this case, homogenization techniques can extract the effective constitutive response at the macroscale from representative simulations at the lower scales. Examples include multiple-level finite-element (FE) analysis or FE^n [30, 56, 70], as well as the homogenization of atomistic ensembles to be used at the material-point level in macroscale FE simulations [15, 16, 62, 73]. By contrast, *concurrent scale-coupling* methods avoid the aforementioned separation of scales and instead integrate different constitutive descriptions into a single-scale model by spatially separating domains treated, e.g., by first-principles, molecular dynamics, discrete defect mechanics, and continuum theories. Prominent examples comprise Coupled Atomistic/Discrete-Dislocation (CADD) models [17, 59, 74] and AtoDis [13], furthermore the Bridging Domain Method (BDM) [12] and Bridging Scale Decomposition [50], as well as Macroscopic, Atomistic, AB Initio Dynamics (MAAD) [2, 14] which couples several scales. In such methods, a key challenge arises from the necessity to pass information across interfaces between different model domains. To pick out one example, CADD is an elegant methodology which embeds a small MD domain into a larger region treated by a Discrete Dislocation (DD) description. Here, the passing of lattice defects across the interface between the two domains is a major challenge. In order to

circumvent such difficulties, *coarse-graining techniques* apply the same lower-scale constitutive description to the entire model but scale up in space and/or in time. Classical examples include Coarse-Grained MD (CGMD) [69] as well as the quasicontinuum (QC) method [82]. We note that, while upscaling in time and in space are equally important, the primary focus here will be on spatial coarse-graining, which is the main achievement of the QC approximation. Upscaling of atomistic simulations in the time domain has been investigated in the context of MD simulations, see, e.g., [41, 89, 90], and can be added to a spatial coarse-graining scheme such as the QC method. A particular QC formulation (applicable to finite temperature) to study, e.g., long-term mass and heat transfer phenomena was introduced recently [6, 88, 91]. The QC approximation relies upon the crystalline structure and is ideally suited to carry out zero-temperature calculations, as presented in the following. A variety of finite-temperature QC extensions exist, see, e.g., [21, 27, 34, 45, 54, 69, 72, 85, 86], which can be applied on top of the presented spatial coarse-graining strategies.

Spatial coarse-graining reduces the number of degrees of freedom by introducing geometric constraints, thereby making the lower-scale accuracy efficiently available for larger-scale simulations [37, 38, 78, 82]. Coarse-graining strategies offer a number of advantages over domain-coupling methods: (1) the model is solely based on the lower-scale constitutive laws and hence comes with superior accuracy (in contrast to coupling methods, there is no need for a separate and oftentimes empirical constitutive law in the continuum region); (2) the transition from fully resolved to coarse-grained regions is seamless (no approximate hand-shake region is required between different domains in general); (3) depending on the chosen formulation, model adaptation techniques can efficiently reduce computational complexity by tying full resolution to those regions where it is indeed required (such as in the vicinity of lattice defects or cracks and voids).

The *quasicontinuum method* was introduced to bridge from atomistics to the continuum by applying finite element interpolation schemes to atoms in a crystal lattice [58, 65, 82]. This is achieved by three integral components: *geometric constraints* (which interpolate lattice site positions from the positions of a reduced set of representative atoms), *summation rules* or *sampling rules* (which avoid the computation of thermodynamic quantities from the full atomistic ensemble), and *model adaptation* schemes (which localize atomistic resolution and thereby efficiently minimize the total number of degrees of freedom). To date, numerous QC flavors have been developed which mainly differ in the choice of how the aforementioned three aspects are realized. Despite their many differences, all QC-based techniques share as a common basis the interpolation of atomic positions from a set of representative atoms as the primary coarse-graining tool.

The family of QC methods has been applied to a wide range of problems of scientific and technological interest such as studies of the interactions of lattice defects in fcc and bcc metals. Typical problems include nanoindentation [48, 51, 83], interactions of lattice defects [35, 65, 76] or of defects with nanosized cracks [36, 68, 80] and nanovoids [6, 66, 98], or with individual interfaces [47, 97]. Beyond metals, the developed modeling techniques can be extended, e.g., to ferroelectric

materials and ionic crystals via electrostatic interactions [20] and multi-lattice approaches [1, 22], further to non-equilibrium thermodynamics [45, 54, 69, 72, 88], also to structural mechanics [7, 9] and two-dimensional materials [64, 92], and in principle to any material system with crystalline order as long as a suitable position-dependent interatomic potential is available.

In this chapter, we will review the common theoretical basis of the family of QC methods, followed by the description of particular QC schemes and available techniques. We then proceed to highlight past and recent applications and extensions of the QC technique to study the mechanics and physics of solids and structures, and we conclude by summarizing some open questions and challenges to be addressed in the future or subject to ongoing research. Since such a book chapter cannot give a full account of all related research, we focus on—in our view—important QC advances and contributions and apologize if we have overlooked specific lines of research. For a list of related publications, the interested reader is also referred to the *qcmethod.org* website maintained by Tadmor and Miller [81].

5.2 The Quasicontinuum Method

The rich family of QC methods is united by the underlying concepts of (1) significantly reducing the number of degrees of freedom by suitable interpolation schemes, and (2) approximating the thermodynamic quantities of interest by summation or sampling rules. Let us briefly outline those concepts before summarizing particular applications and extensions of the QC method.

5.2.1 Representative Atoms and the Quasicontinuum Approximation

In classical mechanics, an atomistic ensemble containing N atoms is uniquely described by how their positions $\mathbf{q} = \{\mathbf{q}_1, \dots, \mathbf{q}_N\}$ and momenta $\mathbf{p} = \{\mathbf{p}_1, \dots, \mathbf{p}_N\}$ with $\mathbf{p}_i = m_i \dot{\mathbf{q}}_i$ evolve with time t . Here and in the following, m_i represents the mass of atom i , and dots denote material time derivatives. Then, the ensemble's total Hamiltonian \mathcal{H} is given by

$$\mathcal{H}(\mathbf{q}, \mathbf{p}) = \sum_{i=1}^N \frac{|\mathbf{p}_i|^2}{2m_i} + V(\mathbf{q}), \quad (5.1)$$

where the first term accounts for the kinetic energy and the second term represents the potential energy of the ensemble with V denoting a suitable atomic interaction potential which we assume to depend on atomic positions only. The time evolution of the system is governed by Hamilton's equations, which yield Newton's equations of motion for all atoms $i = 1, \dots, N$,

$$m_i \ddot{\mathbf{q}}_i = \mathbf{f}_i(\mathbf{q}) = -\frac{\partial V}{\partial \mathbf{q}_i}(\mathbf{q}), \quad (5.2)$$

where $\mathbf{f}_i(\mathbf{q})$ represents the total (net) force acting on atom i . We note that V can, in principle, depend on both positions \mathbf{p} and momenta \mathbf{q} (the latter may be necessary, e.g., when using the quasiharmonic and other approximations for quasistatic finite-temperature formulations without time discretization). For conciseness, we here restrict ourselves to position-dependent potentials only; the extension to include momenta is straightforward. As one of the cornerstones of the QC method, we limit our analysis to crystalline solids in which the ground state atomic positions coincide with sites of a regular lattice described by a set of Bravais vectors that span the discrete periodic array of lattice sites. In most materials (including metals, ceramics, and organic materials), the interaction potential usually allows for an additive decomposition, i.e.

$$V(\mathbf{q}) = \sum_{i=1}^N E_i(\mathbf{q}) \quad (5.3)$$

with E_i being the energy of atom i . Some authors in the scientific literature have preferred to distinguish between external and internal forces by introducing external forces $\mathbf{f}_{i,\text{ext}}$ on all atoms $i = 1, \dots, N$ so that

$$\mathbf{f}_i(\mathbf{q}) = \mathbf{f}_{i,\text{ext}}(\mathbf{q}_i) - \frac{\partial V}{\partial \mathbf{q}_i}(\mathbf{q}). \quad (5.4)$$

Ideally (and in any reasonable physical system), such external forces are conservative and derive from an external potential $V_{\text{ext}}(\mathbf{q})$ and we may combine internal and external forces into a single potential, which is tacitly assumed in the following. Examples of conservative external forces include gravitation, long-range Coulombic interactions, or multi-body interactions such as during contact. For computational convenience, the latter is oftentimes realized by introducing artificial potentials, see, e.g., [40] for an effective external potential for spherical indenters.

Due to limitations of computational resources, it is generally not feasible to apply the above framework to systems that are sufficiently large to simulate long-range elastic effects, even for short-range interatomic potentials. However, except in the vicinity of flaws and lattice defects such as cracks and dislocations, respectively, the local environment of each atom in a crystal lattice is almost identical up to rigid body motion. Therefore, the *QC approximation* replaces the full atomistic ensemble by a reduced set of $N_h \ll N$ representative atoms (often referred to as *repatoms* for short). This process is shown schematically in Fig. 5.2.

Let us denote the repatom positions by $\mathbf{x}(t) = \{\mathbf{x}_1(t), \dots, \mathbf{x}_{N_h}(t)\}$. The approximate current positions \mathbf{q}_i^h and momenta \mathbf{p}_i^h of all atoms $i = 1, \dots, N$ are now obtained from interpolation, i.e. we have

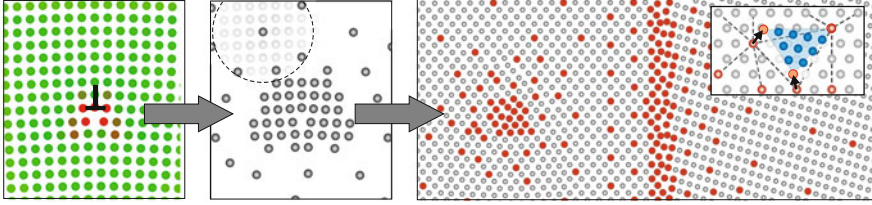


Fig. 5.2 Illustration of the QC methodology: identification of atoms of interest (e.g., high-centrosymmetry lattice sites near a dislocation core), reduction to the set of repatoms (coarsening the full atomic lattice by choosing a small set of representative atomic sites), and the interpolation of atomic positions (*blue* in the small *inset*) from repatom positions (*red*) with an example repatom distribution around a dislocation and a grain boundary in two dimensions

$$\mathbf{q}_i \approx \mathbf{q}_i^h = \sum_{a=1}^{N_h} N_a(\mathbf{X}_i) \mathbf{x}_a \quad (5.5)$$

and consequently

$$\mathbf{p}_i \approx \mathbf{p}_i^h = m_i \dot{\mathbf{q}}_i^h = m_i \sum_{a=1}^{N_h} N_a(\mathbf{X}_i) \dot{\mathbf{x}}_a. \quad (5.6)$$

$N_a(\mathbf{X}_i)$ is the shape function of repatom a evaluated at the position \mathbf{X}_i of lattice site i in the undeformed (reference) configuration (analogously to shape functions commonly used in the finite element method). As an essential feature, one usually requires this coarse-graining scheme to locally recover the exact atomic ensemble when all atoms are turned into repatoms; i.e., if every lattice site is a repatom, then we should recover full atomistics exactly. In other words, in the atomistic limit we require $\mathbf{q}_i = \mathbf{x}_i$. This in turn implies that shape functions should be chosen to satisfy the Kronecker property, i.e., $N_a(\mathbf{X}_b) = \delta_{ab}$ for all $1 \leq a, b \leq N_h$ with δ_{ij} denoting Kronecker's delta ($\delta_{ij} = 1$ if $i = j$ and 0 otherwise). This is the case, e.g., for Lagrange interpolation functions (including affine interpolation), which ensure that shape functions are 1 at their respective node and 0 at all other nodes.

By borrowing concepts from the finite element method, the above geometric constraints within the original QC method [42, 71, 82] made use of an affine interpolation on a Delaunay-triangulated mesh. More recent versions have explored higher-order polynomial shape functions [46, 63] as well as meshless interpolations using smoothed-particle approaches [94, 96] or local maximum-entropy shape functions [43].

The introduction of the geometric constraints in (5.5) has reduced the total number of independent degrees of freedom from $d \times N$ in d dimensions to $d \times N_h$. Therefore, the approximate Hamiltonian \mathcal{H}^h of the coarse-grained system, now involving approximate atomic positions $\mathbf{q}^h = \{\mathbf{q}_1^h, \dots, \mathbf{q}_N^h\}$ and momenta $\mathbf{p}^h = \{\mathbf{p}_1^h, \dots, \mathbf{p}_N^h\}$, only depends on the positions and momenta of the repatoms through (5.5):

$$\mathcal{H}^h(\mathbf{x}, \dot{\mathbf{x}}) = \sum_{i=1}^N \frac{|\mathbf{p}_i^h|^2}{2m_i} + V(\mathbf{q}^h). \quad (5.7)$$

Instead of solving for the positions and momenta of all N lattice sites, the QC approximation allows us to update only the positions and momenta of the N_h repatoms, which requires to compute forces on repatoms. These are obtained from the potential energy by differentiation, which yields the net force on repatom k :

$$\mathbf{F}_k(\mathbf{x}) = -\frac{\partial V(\mathbf{q}^h)}{\partial \mathbf{x}_k} = \sum_{j=1}^N \mathbf{f}_j^h(\mathbf{q}^h) N_k(\mathbf{X}_j) \quad (5.8)$$

with

$$\mathbf{f}_j^h(\mathbf{q}^h) = -\frac{\partial V(\mathbf{q}^h)}{\partial \mathbf{q}_j^h} = -\sum_{i=1}^N \frac{\partial E_i(\mathbf{q}^h)}{\partial \mathbf{q}_j^h}, \quad (5.9)$$

the total force acting on atom j . It is important to note that, in an infinite Bravais lattice (i.e., in a defect-free single-crystal in the absence of external loading or free surfaces), the forces on all atoms vanish, i.e. we have $\mathbf{f}_i^h(\mathbf{q}^h) = \mathbf{0}$, so that the net forces on all repatoms vanish as well ($\mathbf{F}_k = \mathbf{0}$).

5.2.2 Summation Rules and Spurious Force Artifacts

Summation rules have become an integral ingredient of all QC methods (even though they are sometimes not referred to as such). Although the above introduction of repatoms has reduced the total number of degrees of freedom significantly from $d \times N$ to $d \times N^h$, the calculation of repatom forces still requires computing the forces between all N atoms and their on average N_b neighbors located within each atom's radius of interaction. These $\mathcal{O}(N \times N_b)$ operations become computationally not feasible for realistically sized systems. We note that, in principle, summations in (5.8) can be reduced to the support of the shape functions (i.e., to regions in which $N_k(\mathbf{X}_j) \neq 0$) but even this is prohibitively expensive in regions of dilute repatom concentrations. Therefore, *summation rules* or *sampling rules* have been introduced to approximate the thermodynamic quantities of interest of the full atomistic ensemble by those of a small set of carefully chosen lattice sites (in the following referred to as *sampling atoms*), comparable to quadrature rules commonly found in the finite element method.

QC summation rules have either approximated the energy of the system (so-called *energy-based QC*) [5, 28] or the forces experienced by the repatoms (*force-based QC*) [42]. Within each of those two categories, multiple versions have been proposed. Here, we will first describe what is known as *fully nonlocal* energy-based

and force-based QC formulations and then extract the original *local/nonlocal* QC method as a special case of energy-based QC.

5.2.2.1 Energy-Based QC

In energy-based nonlocal QC formulations, the total Hamiltonian is approximated by a weighted sum over a carefully selected set of *sampling atoms* (which do not have to coincide with the repatoms introduced above). To this end, we replace the sum over index i in (5.3) or (5.8) by a weighted sum over N_s carefully-chosen sampling atoms, see, e.g., [5, 28, 29]. Consequently, the total potential energy is approximated by

$$V(\mathbf{q}^h) = \sum_{i=1}^N E_i(\mathbf{q}^h) \approx \tilde{V}(\mathbf{q}^h) = \sum_{\alpha=1}^{N_s} w_\alpha E_\alpha(\mathbf{q}^h), \quad (5.10)$$

where w_α is the weight of sampling atom α . Physically, w_α denotes the number of lattice sites represented by sampling atom α .

The force experienced by repatom k is obtained by differentiation in analogy to (5.8):

$$\tilde{\mathbf{F}}_k(\mathbf{x}) = -\frac{\partial \tilde{V}(\mathbf{q}^h)}{\partial \mathbf{x}_k} = -\sum_{\alpha=1}^{N_s} w_\alpha \sum_{j=1}^N \frac{\partial E_\alpha(\mathbf{q}^h)}{\partial \mathbf{q}_j^h} N_k(\mathbf{X}_j). \quad (5.11)$$

Now, repatom force calculation has been reduced to $\mathcal{O}(N_s \times N_b)$ operations (accounting for the fact that the sum over j above effectively only involves N_b neighbors within the potential's cutoff radius). The selection of sampling atoms and the calculation of sampling atom weights aim for a compromise between maximum accuracy (ideally $N_s = N$ and $w_\alpha = 1$) and maximum efficiency (requiring $N_s \ll N$ and $w_\alpha \gg 1$).

In order to seamlessly bridge from atomistics to the continuum without differentiating between atomistic and coarse-grained regions, the above summation rules can be interpreted as a fully *nonlocal QC* approximation which treats the entire simulation domain in the same fashion. Summation rules now differ by the choice of (1) sampling atom locations and (2) sampling atom weights. Successful examples of summation rules introduced previously include *node-based cluster summation* [42] with sampling atoms located in clusters around repatoms, and *quadrature-type summation* [33] with sampling atoms chosen nearest to Gaussian quadrature points with or without the repatoms included as sampling atoms. Furthermore, *element-based summation rules* have been introduced in the nonlocal QC context [33, 95] and have demonstrated superior accuracy over traditional cluster-based summation schemes [37]. Recently, a *central summation rule* was proposed in [11] as an ad-hoc compromise between local and quadrature summation rules, which is similar in

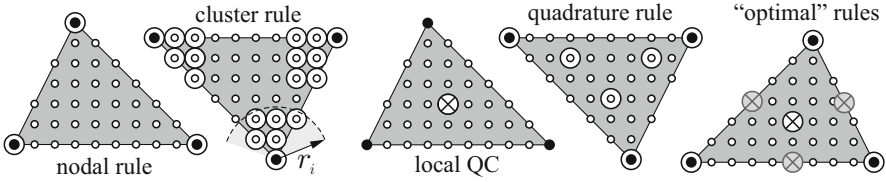


Fig. 5.3 Illustration of popular summation rules with *small open circles* denoting lattice sites, *solid circles* representing repatoms, and *large open circles* are sampling atoms (*crossed circles* denote sampling atoms whose neighborhoods undergo affine deformations). Optimal summation rules [5] are shown of first and second order (the *gray* sampling atoms only exist in the second-order rule)

spirit and contained as a special case within the optimal summation rules recently introduced in [5]. Figure 5.3 illustrates some of the most popular summation rules.

Many summation rules were introduced in an ad-hoc manner to mitigate particular QC deficiencies (e.g., cluster rules were introduced to remove zero-energy modes in force-based QC [42]) or by borrowing schemes from related models (e.g., finite element quadrature rules [33]). The recent *optimal sampling rules* [5] followed from optimization and ensure small or vanishing force artifacts in large elements while seamlessly bridging to full atomistics. Their new second-order scheme also promises superior accuracy when modeling free surfaces and associated size effects at the nanoscale [4].

5.2.2.2 Force Artifacts

Summation rules on the energy level not only reduce the computational complexity but they also give rise to *force artifacts*, see, e.g., [5, 28] for reviews within the energy-based context. By rewriting (5.11) without neighborhood truncations as

$$\tilde{\mathbf{F}}_k(\mathbf{x}) = - \sum_{\alpha=1}^{N_s} w_{\alpha} \sum_{j=1}^N \frac{\partial E_{\alpha}(\mathbf{q}^h)}{\partial \mathbf{q}_j^h} N_k(\mathbf{X}_j) = \sum_{j=1}^N \left(- \sum_{\alpha=1}^{N_s} w_{\alpha} \frac{\partial E_{\alpha}(\mathbf{q}^h)}{\partial \mathbf{q}_j^h} \right) N_k(\mathbf{X}_j), \quad (5.12)$$

and comparing with (5.8), we see that the term in parentheses in (5.12) is not equal to force \mathbf{f}_j^h and hence does not vanish in general even if $\mathbf{f}_j^h = \mathbf{0}$ for all atoms (unless we choose all atoms to be sampling atoms, i.e., unless $N_s = N$ and $w_{\alpha} = 1$). As a consequence, the QC representation with energy-based summation rules shows what is known as *residual forces* in the undeformed ground state which are non-physical.

In uniform QC meshes (i.e. uniform repatom spacings, uniform sampling atom distribution, and a regular mesh), these residual forces indeed disappear due to symmetry; specifically, the sum in parentheses in (5.12) cancels pairwise when carrying out the full sum. Residual forces hence appear only in spatially non-uniform meshes, see also [37] for a discussion. In general, one should differentiate

between residual and spurious forces [5, 28]. Here, we use the term *residual force* to denote force artifacts arising in the undeformed configuration. In an infinite crystal, these can easily be identified by computing all forces in the undeformed ground state. However, force errors vary nonlinearly with reatom positions. Therefore, we speak of *spurious forces* when referring to force artifacts in the deformed configuration. As shown, e.g., in [5], correcting for residual forces by subtracting those as dead loads does not correct for spurious forces and can lead to even larger errors in simulations. Indeed, in many scenarios this dead-load correction is not easily possible since the undeformed ground state may contain, e.g., free surfaces. In this case, the computed forces in the undeformed ground state contain both force artifacts and physical forces. Thus, without running a fully atomistic calculation for comparison, it is impossible to differentiate between residual force artifacts and physical forces arising, e.g., due to surface relaxation [4]. Even though residual and spurious forces are conservative in the energy-based scheme, they are non-physical and can drive the coarse-grained system into incorrect equilibrium states. Special correction schemes have been devised which effectively reduce or remove the impact of force artifacts, see, e.g., the *ghost force correction* techniques in [71, 75]. However, such schemes require a special algorithmic treatment at the interface between full resolution and coarse-grained regions, which may create computational difficulties and, most importantly, requires the notion of an interface.

Based on mathematical analyses, further energy-based schemes have been developed, which blend atomistics and coarse-grained descriptions by a special formulation of the potential energy or the reatom forces. Here, an interfacial domain between full resolution and coarse regions is introduced, in which the thermodynamic quantities of interest are taken as weighted averages of the exact atomistic and the approximate coarse-grained ones [49, 53]. Such a formulation offers clear advantages, including the avoidance of force artifacts. It also requires the definition of an interface region, which may be disadvantageous in a fully nonlocal QC formulation with automatic model adaption since no notion of such interfaces may exist strictly [5].

5.2.2.3 Force-Based QC

In order to avoid force artifacts, *force-based summation rules* were introduced in [42]. These do not approximate the Hamiltonian but the reatom forces explicitly. Ergo, the summation rule is applied directly to the reatom forces in (5.8), viz.

$$\mathbf{F}_k(\mathbf{x}) = \sum_{i=1}^N \mathbf{f}_i^h(\mathbf{q}^h) N_k(\mathbf{X}_i) \approx \tilde{\mathbf{F}}_k(\mathbf{x}) = \sum_{\alpha=1}^{N_s} w_\alpha \mathbf{f}_\alpha^h(\mathbf{q}^h) N_k(\mathbf{X}_\alpha). \quad (5.13)$$

As a consequence, this force-based formulation does not produce residual forces because $\mathbf{f}_\alpha^h(\mathbf{q}^h) = \mathbf{0}$ in an undeformed infinite crystal. The same holds true for an

infinite crystal that is affinely deformed: for reasons of symmetry the repatom forces cancel, and spurious force artifacts are effectively suppressed.

Yet, this approximation gives rise to a new problem: the force-based method is non-conservative; hence, there is no potential from which repatom forces derive. This has a number of drawbacks, as discussed, e.g., in [28, 37, 57]. In quasistatic problems, the non-conservative framework may lead to slow numerical convergence, cause numerical instability, or converge to non-physical equilibrium states, see, e.g., the analyses in [24–26, 52, 61]. Furthermore, for dynamic or finite-temperature scenarios, a QC approximation using force-based summation rules cannot be used to simulate systems in the microcanonical ensemble (where the system’s energy is to be conserved; other ensembles may, of course, be used). Finally, repatom masses, required for dynamic simulations, are not uniquely defined because there is no effective kinetic energy potential when using force-based summation rules (see also Sect. 5.2.2.5 below). In contrast, energy-based summation rules lead to conservative forces and to strictly symmetric stiffness matrices with only the six admissible zero eigenvalues [28]. Moreover, the proper convergence of energy-based QC techniques was shown recently for harmonic lattices [29].

5.2.2.4 Local/Nonlocal QC

The original QC method of [82] uses affine interpolation within elements and may be regarded as a special energy-based QC scheme, in which atomistic and coarse-grained regions are spatially separated. In the atomistic region and its immediate vicinity, the full atomistic description is applied and one solves the discrete (static) equations of motion for each atom and approximations thereof near the interface (*nonlocal QC*). In the coarse-grained region, a particular element-based summation rule is employed (*local QC*): for each element, the energy is approximated by assuming an affine deformation of all atomic neighborhoods within the element, so that one Cauchy Born-type sampling atom per element is sufficient and the total potential energy is the weighted sum over all such element energies. This concept has been applied successfully to a myriad of examples, primarily in two dimensions (or in 2.5D by assuming periodicity along the third dimension). Since the element-based summation rule in the nonlocal coarse region produces no force artifacts [5], force artifacts here only appear at the interface between atomistic and coarse-grained regions and have traditionally been called *ghost forces* [58, 71]. For a comprehensive comparison of this technique with other atomistic-to-continuum-coupling techniques, see [57]. Figure 5.4 schematically illustrates the concepts of local/nonlocal and fully nonlocal QC.

5.2.2.5 Repatom Masses

Besides repatom forces, energy-based summation rules provide consistent repatom masses, as mentioned above. When approximated by the QC interpolation scheme,

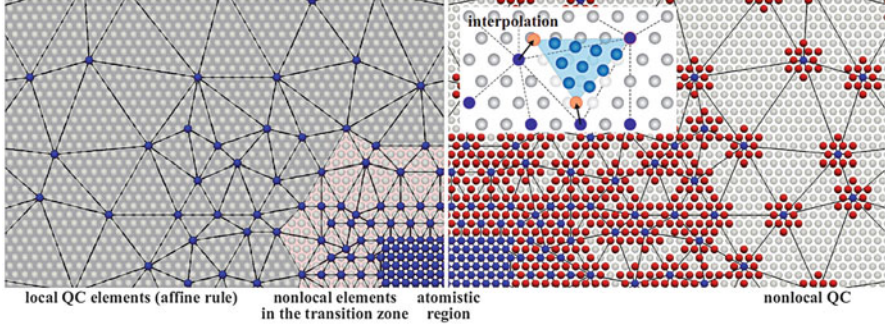


Fig. 5.4 Schematic view of the local/nonlocal (*left*) and fully nonlocal (*right*) QC formulations. The shown nonlocal scheme uses a node-based cluster summation rule. The *inset* on the right illustrates the affine interpolation of atomic positions from reptoms, which is the same in both formulations

the total kinetic energy of an atomic ensemble becomes

$$\begin{aligned}
 \frac{1}{2} \sum_{i=1}^N m_i (\dot{\mathbf{q}}_i^h)^2 &= \frac{1}{2} \sum_{i=1}^N m_i \left| \sum_{a=1}^{N_h} N_a(X_i) \dot{\mathbf{x}}_a \right|^2 \\
 &= \frac{1}{2} \sum_{a=1}^{N_h} \sum_{c=1}^{N_h} \dot{\mathbf{x}}_a \cdot \left(\sum_{i=1}^N m_i N_a(X_i) N_c(X_i) \right) \dot{\mathbf{x}}_c,
 \end{aligned} \tag{5.14}$$

where the term in parentheses may be interpreted as the components M_{ac}^h of a consistent mass matrix \mathbf{M}^h . In avoidance of solving a global system during time stepping, one often resorts to mass lumping in order to diagonalize \mathbf{M}^h . Applying the energy-based summation rule to the total Hamiltonian (and thus to the kinetic energy) yields a consistent approximation of the kinetic energy with mass matrix components

$$M_{ac}^h = \sum_{i=1}^N m_i N_a(X_i) N_c(X_i) \approx \tilde{M}_{ac}^h = \sum_{b=1}^{N_s} w_b m_b N_a(X_b) N_c(X_b). \tag{5.15}$$

In case of mass matrix lumping, the equations of motion of all reptoms now become

$$\tilde{m}_k^h \ddot{\mathbf{x}}_k = \tilde{\mathbf{F}}_k(\mathbf{x}), \tag{5.16}$$

which can be solved by (explicit or implicit) finite difference schemes. The calculation of reptom masses is of importance not only for dynamic QC simulations, but it is also relevant in quasistatic finite-temperature QC formulations.

5.2.2.6 Example: Embedded Atom Method

The QC approximation outlined above is sufficiently general to model the performance of most types of crystalline solids, as long as their potential energy can be represented as a function of atomic positions. Let us exemplify the general concept by a frequently used family of interatomic potentials for metals (which has also been used most frequently in conjunction with the QC method). The embedded atom method (EAM) [19] defines the interatomic potential energy of a collection of N atoms by

$$E_i(\mathbf{q}) = \frac{1}{2} \sum_{j \neq i} \Phi(r_{ij}) + \mathcal{F}(\rho_i), \quad \rho_i = \sum_{j \neq i} f(r_{ij}). \quad (5.17)$$

The pair potential $\Phi(r_{ij})$ represents the energy due to electrostatic interactions between atom i and its neighbor j , whose distance r_{ij} is the norm of the distance vector $\mathbf{r}_{ij} = \mathbf{q}_i - \mathbf{q}_j$. ρ_i denotes an effective electron density sensed by atom i due to its neighboring atoms. $f(r_{ij})$ is the electron density at site i due to atom j as a function of their distance r_{ij} . $\mathcal{F}(\rho_i)$ accounts for the energy release upon embedding atom i into the local electron density ρ_i . From (5.2), the exact force \mathbf{f}_k acting on atom k is obtained by differentiation, viz.

$$\mathbf{f}_k(\mathbf{q}) = - \sum_{i=1}^N \frac{\partial E_i(\mathbf{q})}{\partial \mathbf{q}_k} = - \sum_{j \in n_l(k)}^N [\Phi'(r_{kj}) + \{\mathcal{F}'(\rho_k) + \mathcal{F}'(\rho_j)\} f'(r_{kj})] \frac{\mathbf{r}_{kj}}{r_{kj}}. \quad (5.18)$$

Since most (non-ionic) potentials are short-range (in particular those for metals), one can efficiently truncate the above summations to include only neighboring atoms within the radius of interaction ($n_l(i)$ denotes the set of neighbors within the sphere of interaction of atom i). Introducing the QC approximation along with an energy-based summation rule now specifies the approximate repatom force as

$$\tilde{\mathbf{F}}_k(\mathbf{x}) = - \sum_{\alpha=1}^{N_s} w_\alpha \sum_{j \in n_l(\alpha)} \left[\frac{1}{2} \Phi'(r_{\alpha j}^h) + \mathcal{F}'(\rho_\alpha^h) f'(r_{\alpha j}^h) \right] \frac{\mathbf{r}_{\alpha j}^h}{r_{\alpha j}^h} [N_k(\mathbf{X}_\alpha) - N_k(\mathbf{X}_j)], \quad (5.19)$$

which completes the coarse-grained description required for QC simulations. Note that, as discussed above, repatom forces (5.19) are prone to produce residual and spurious force artifacts in non-uniform QC meshes.

5.2.2.7 Adaptive Refinement

One of the general strengths of the QC method is its suitability for adaptive model refinement. This is particularly useful when there is no a-priori knowledge about

where within a simulation domain atomistic resolution will be required during the course of a simulation. For example, when studying defect mechanisms near a crack tip or around a pre-existing lattice defect, it may be sufficient to restrict full atomistic resolution to regions in the immediate vicinity of those microstructural features and efficiently coarsen away from those. However, when investigating many-defect interactions or when the exact crack path during ductile failure is unknown, it is beneficial to make use of automatic model adaptation. By locally refining elements down to the full atomistic limit, full resolution can effectively be tied to evolving defects in an efficient manner. In the fully nonlocal QC method [5], this transition is truly seamless as there is no conceptual differentiation between atomistic and coarse domains. In the local/nonlocal QC method as well as in blended QC formulations the transition is equally possible but may require a special algorithmic treatment.

Mesh refinement requires two central ingredients: a criterion for refinement and a geometric refinement algorithm. The former can be realized on the element level, e.g., by checking invariants of the deformation gradient within each element and comparing those to a threshold for refinement [42]. Alternatively, one can introduce criteria based on repeatoms or sampling atoms, e.g., by checking the energy or the centrosymmetry of repeatoms or sampling atoms and comparing those to refinement thresholds. The most common geometric tool is element bisection; however, a large variety of tools exist and these are generally tied to the specifically chosen interpolation scheme.

Unlike in the finite element method, mesh adaptation within the QC method is challenging since element vertices, at least in the most common implementations, are restricted to sites of the underlying Bravais lattice (this ensures that full atomistics is recovered upon ultimate refinement). The resulting constrained mesh generation and adaptation has been discussed in detail, e.g. in [3]. While mesh refinement is technically challenging but conceptually straightforward, mesh coarsening presents a bigger challenge. Meshless formulations [43, 94, 96] appear promising but have not reached sufficient maturity for large-scale simulations.

5.2.3 Features and Extensions

The QC methods described above have been applied to a variety of scenarios which go beyond the traditional problem of quasistatic equilibration at zero-temperature. In particular, QC extensions have been proposed in order to describe phase transformations and deformation twinning, finite temperature, atomic-level heat and mass transfer, or ionic interactions such as in ferroelectrics. In addition, the basic concept of the QC method has been applied to coarse-grain discrete mechanical systems beyond atomistics. Here, we give a brief (non-exhaustive) summary of such special QC features and extensions.

5.2.3.1 Multilattices

The original (local) QC approximation applies an affine interpolation to all lattice site positions within each element in the coarse domain, which results in affine neighborhood changes within elements (the same applies to the optimal summation rules within fully nonlocal QC). By using Cauchy–Born (CB) kinematics, one can account for relative shifts within the crystalline unit cells such as those occurring during domain switching in ferroelectrics or during solid-state phase transitions and deformation twinning. The CB rule is thus used in coarse-grained regions to relate atomic motion to continuum deformation gradients. In order to avoid failure of the CB kinematics, such a multilattice QC formulation has been augmented with a phonon stability analysis which detects instability and identifies the minimum required periodic cell size for subsequent simulations. This augmented approach has been referred to as *Cascading Cauchy–Born Kinematics* [23, 77] and has been applied, among others, to ferroelectrics [84] and shape-memory alloys [23].

5.2.3.2 Finite Temperature and Dynamics

Going from zero to finite temperature within the QC framework is a challenge that has resulted in various approximate descriptions but has not been resolved entirely. In contrast to full atomistics, the physical behavior of continua is generally governed by thermodynamic state variables such as temperature and by thermodynamic quantities such as the free energy. Therefore, many finite-temperature QC frameworks have constructed an effective, temperature-dependent free energy potential; for example, see [27, 34, 45, 54, 72, 85, 86]. Dynamic simulations of finite-temperature and non-equilibrium processes raise additional questions. Here, we discuss a few representative finite-temperature QC formulations (often referred to as *hotQC* techniques); for reviews, see also [44, 85, 87, 88] and the references therein, to name but a few.

Within the local/nonlocal QC framework, finite-temperature has often been enforced in different ways in the atomistic and the continuum regions, see, e.g., [85]. While in the atomistic region a thermostat can be used to maintain a constant temperature, an effective, temperature-dependent free energy is formulated in the coarse domain, e.g., based on the *quasiharmonic approximation* [85]. For quasistatic equilibrium calculations, the dynamic atomistic ensemble is then embedded into the static continuum description of the coarse-grained model. Alternatively, in dynamic hotQC simulations of this type, all repatoms (including those in both regions) evolve dynamically. The quasiharmonic approximation was shown to be well suited to describe, e.g., the volumetric lattice expansion at moderate temperatures (where the phonon-based model serves as a leading-order approximation). Drawbacks include the inaccuracy observed at elevated temperature levels. Computational drawbacks in terms of instability or technical difficulties may arise from the necessity to compute up to third-order derivatives of the interatomic potentials. These must hence be sufficiently smooth but often derive from piece-wise polynomials or tabulated values in reality.

Temperature and *dynamics* are intimately tied within any framework based on atomistics. In principle, the zero-temperature QC schemes described in previous sections can easily be expanded into dynamic calculations by accounting for inertial effects and solving the dynamic equations of motion instead of their static counterparts. In non-uniform QC meshes, however, this inevitably leads to the reflection and refraction of waves at mesh interfaces and within non-uniform regions. While such numerical artifacts may be of limited concern within, e.g., the finite element method, they become problematic in the present atomistic scenario, since atomic vibrations imply heat. For example, when high-frequency, short-wavelength signals cannot propagate into the coarse region, the fully refined region will trap high-frequency motion, which leads to artificial heating of the atomistic region and thus to non-physical simulation artifacts. Dynamic finite-temperature QC techniques hence face the challenge of removing such artifacts.

Any dynamic atomistic simulation must cope with the small time steps on the order of femtoseconds, which are required for numerical stability of the explicit finite difference schemes. This, of course, also applies to QC. In general, techniques developed for the acceleration of MD can also be applied to the above QC framework. One such example, *hyperQC* [41] borrows concepts of the original hyperdynamics method [89] and accelerates atomistic calculations by energetically favoring rare events through the modification of the potential energy landscape. This approach was reported as promising in simple benchmark calculations [41].

As a further example, finite-temperature QC has been realized by the aid of *Langevin thermostats* [54, 87]. Here, the QC approximation is applied within the framework of dissipative Lagrangian mechanics with a viscous term that expends the thermal energy introduced by a Langevin thermostat through a random force at the repatom level. In a nutshell, the repatoms can be pictured as an ensemble of nodes suspended in a viscous medium which represents the neglected degrees of freedom. The effect of this medium is approximated by frictional drag on the repatoms as well as random fluctuations from the thermal motion of solvent particles. As a consequence, high-frequency modes (i.e., phonons) not transmitted across mesh interfaces are dampened out by the imposed thermostat in order to sample stable canonical ensemble trajectories. This method is anharmonic and was used to study non-equilibrium, thermally activated processes. Unfortunately, the reduced phonon spectra in the coarse-grained domains result in an underestimation of thermal properties such as thermal expansion. For a thorough discussion, see [87].

In contrast to the above finite-temperature QC formulations which interpret continuum thermodynamic quantities as atomistic time averages, one may alternatively assume ergodicity and take advantage of averages in phase space. This forms the basis of the *maximum-entropy* hotQC formulation [44, 45, 87]. By recourse to mean-field theory and statistical mechanics, this hotQC approach is based on the assumption of maximizing the atomistic ensemble's entropy. To this end, repatoms are equipped with an additional degree of freedom which describes their mean vibrational frequency and which must be solved for in addition to the repatom positions at a given constant temperature of the system. This approach seamlessly bridges across scales and does not conceptually differentiate between atomistic and continuum domains. As described in the following section, this concept has also been extended to account for heat and mass transfer [66, 88].

5.2.3.3 Heat and Mass Transfer

The aforementioned maximum-entropy framework has been applied to study not only finite-temperature equilibrium mechanics but has also been extended to describe non-equilibrium heat and mass transfer in coarse-grained crystals. As explained above, the motion of each atom can be decomposed into high-frequency oscillations (i.e., heat) and its mean path (slow, long-term motion). The principle of maximum entropy along with variational mean-field theory provides the tools to apply this concept to the QC method by providing governing equations for the repatom positions as well as their vibrational frequencies [45, 87, 88]. In addition, the same framework is suitable to describe multi-species systems by equipping repatoms with additional degrees of freedom that represent the local chemical composition. For an atomistic ensemble, this yields an effective total Hamiltonian [66, 87, 88]

$$\mathcal{H}_{\text{eff}}(\bar{\mathbf{q}}, \bar{\mathbf{p}}, \boldsymbol{\omega}) = \sum_{i=1}^N \left\{ \frac{|\bar{\mathbf{p}}_i|^2}{2m_i} + \langle V_i \rangle(\bar{\mathbf{q}}, \bar{\mathbf{p}}, \boldsymbol{\omega}, \mathbf{x}) + 3k_B \theta_i \left[\frac{3}{2}N + \log \left(\frac{\hbar \omega_i}{k_B \theta_i} \right) - 1 + \sum_k^n x_{ik} \log x_{ik} \right] \right\}, \quad (5.20)$$

where $\langle \cdot \rangle$ denotes the phase-space average to be computed, e.g., by numerical quadrature; the associated probability distribution and partition function are available in closed form [88]. N , k_B , and \hbar are the total number of atoms, Boltzmann's and Planck's constants, respectively. ω_i represents the vibrational frequency of atom i , and θ_i is its absolute temperature. In addition to obtaining Hamilton's equations of motion for the mean positions $\bar{\mathbf{q}}(t)$ and momenta $\bar{\mathbf{p}}(t)$ of all N atoms, minimization of the above Hamiltonian also yields the vibrational frequencies ω_i as functions of temperature. In order to describe n different species, x_{ik} denotes the effective molar fraction of species k at atomic site i (i.e., for full atomistics it is either 1 or 0, in the coarse-grained context it will assume any value $x_{ik} \in [0; 1]$). m_i is an effective atomic mass. In addition to interpolating (mean) atomic positions and momenta as in the traditional QC method, one now equips repatoms with vibrational frequencies and molar fractions as independent degrees of freedom to be interpolated: $(\bar{\mathbf{q}}, \bar{\mathbf{p}}, \boldsymbol{\omega}, \mathbf{x})$. While governing equations for atomic positions follow directly, the modeling of heat and mass transfer requires (empirical) relations for atomic-level mass and heat exchange to complement the above framework [88].

We note that the evaluation of the above Hamiltonian requires effective interatomic potentials for many-body ensembles with known average molar fractions x_{ik} . Possible choices include empirical EAM potentials [31, 39] and related lower-bound approximations [88] as well as DFT-informed EAM potentials [67, 93].

5.2.3.4 Ionic Crystals

Ionic interactions, such as those arising, e.g., in solid electrolytes or in complex oxide ferroelectric crystals, present an additional challenge for the QC method because atomic interactions cease to be short-range. The QC summation or sampling rules take advantage of short-range interatomic potentials which admit the local evaluation of thermodynamic quantities of interest, ideally at the element level. When long-range interactions gain importance, that concept no longer applies and new effective summation schemes must be developed such as those reported in [55].

5.2.3.5 Beyond Atomistics

The QC approximation is a powerful tool whose application is not necessarily restricted to atomistic lattices. In general, any periodic array of interacting nodes can be coarsened by a continuum description which interpolates the full set of nodal positions from a small set of representative nodes. Therefore, since its original development for coarse-grained atomistics, the QC method has been extended and applied to various other fields.

As an example at even lower length scales, coarse-grained formulations of *Density Functional Theory* have been reported [32, 79], which considerably speed up electronic calculations. While the key concepts here appertain to the particular formulation of quantum mechanics based on electron densities, the coarse-graining of the set of atomic nuclei may be achieved by recourse to the QC method.

As a further example at larger scales, the QC method can also be applied at the meso- and macroscales in order to coarse-grain periodic structures such as truss or fiber networks. Here, interatomic potentials are replaced by the discrete interactions of truss members or fibers, and the collective response of large networks is again approximated by the selection of representative nodes and suitable interpolation schemes. This methodology was applied to truss lattices [7, 9, 10] and electronic textiles [8]. As a complication, nodal interactions in those examples are not necessarily elastic, so that internal variables must be introduced to account for path dependence in the nodal interactions and dissipative potentials can be introduced based on the virtual power theorem or variational constitutive updates. Figure 5.5 shows a schematic of the coarse-graining of truss lattices as well as the simulated failure of a coarse-grained periodic truss structure loaded in three-point bending. Detailed results will be shown in Sect. 5.3.3.

5.2.4 Codes

A variety of QC codes are currently being used around the world, most of which are owned and maintained by individual research groups. The most prominent and freely available simulation software is the Fortran-based code developed

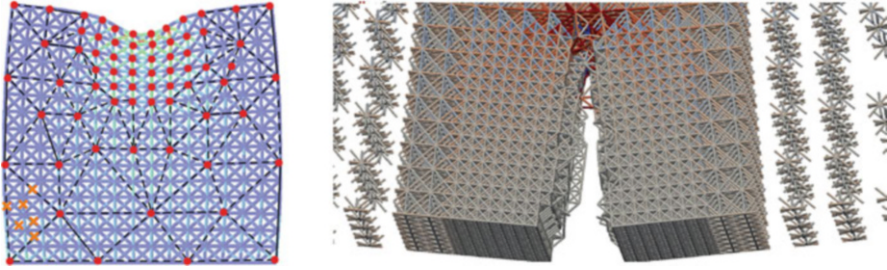


Fig. 5.5 Schematic view of a coarse-grained truss network undergoing indentation (*left*; shown are truss members, nodes, representative nodes, and example sampling truss members within one element) and the simulation result of a truss lattice fracturing during three-point bending (*right*, color-coded by the axial stress within truss members which are modeled as elastic-plastic)

and maintained by Tadmor et al. [81]. This framework is currently restricted to 2.5D simulations and has been used successfully for numerous studies of defect interactions and interface mechanics at the nanoscale [81]. The code is available through the website [81], which also includes a list of references to examples and applications. High-performance codes for 3D QC simulations exist primarily within academic research groups; these include, among others, those of M. Ortiz, P. Ariza, I. Romero et al. (hotQC), J. Knap, J. Marian, and others (force-based QC), E. Tadmor et al. (the 3D extension of [81]), and the authors (fully nonlocal 2D and 3D QC). This is, of course, a non-exhaustive summary of current codes.

5.3 Applications

It is a difficult task to summarize all applications of the QC method to date; for a thorough overview, the interested reader is referred to the QC references found in [81]. Without claiming completeness, the following topics have attracted significant interest in the QC community (for references, see [81]):

- size effects and deformation mechanisms during nanoindentation,
- nanoscale contact and friction, nanoscale scratching and cutting processes,
- interactions between dislocations and grain boundaries (GBs), GB mechanisms,
- phase transformations and deformation twinning, shape-memory alloys,
- fracture and damage in fcc/bcc metals and the brittle-to-ductile transition,
- void and cavity growth at zero and finite temperature,
- deformation and failure mechanisms in single-, bi-, and polycrystals, in particular the mechanics of nanocrystalline solids,
- crystalline sheets and rods, including graphene and carbon nanotubes,
- ferroelectrics and polarization switching,
- electronic textile, fiber networks and truss structures.

In the following sections, we will highlight specific applications of the QC method applied to fcc metals and truss structures. The benchmark examples have been simulated by the authors' fully nonlocal, massively parallel 3D QC code.

5.3.1 Nanoindentation

Nanoindentation is one of the most classical examples that has been studied by the QC method since its inception due to the relatively simple problem setup and the rich inelastic deformation mechanisms that can be observed. Oftentimes, the indenter is conveniently modeled by an external potential [40], which avoids the handling of contact and the presence of two materials.

As an illustrative example of the nonlocal QC method, Fig. 5.6 shows the results of a virtual indentation test into single-crystalline pure copper with a spherical indenter of radius 5 nm up to a maximum indentation depth of 3 nm.

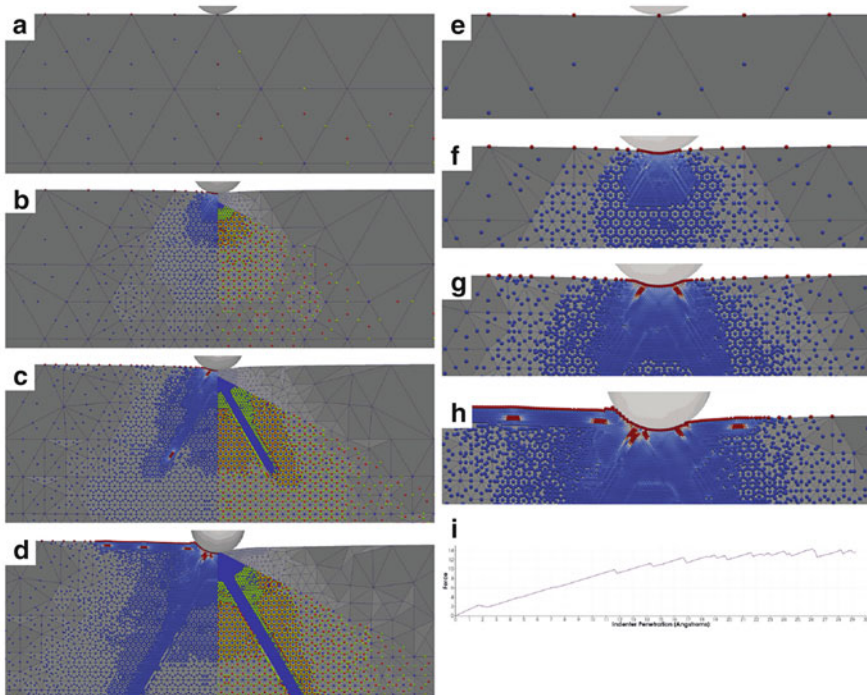


Fig. 5.6 Nanoindentation into a Cu single-crystal: (a)–(d) show the distribution of reptatoms in blue (bottom left panels) as well as color-coded by centrosymmetry (top left panels), the sampling atoms of the first- and second-order summation rules of [5] (shown in red and green, respectively, in the bottom right panels), and the mesh (top right panels). (e)–(h) are zooms of (a)–(d) illustrating the sampling atom centrosymmetry. (i) shows the force-indentation curve (force in eV/Å)

All nanoindentation simulations were performed at an indentation rate of $7.8 \cdot 10^8$ at zero temperature, using an extended Finnis–Sinclair potential [18]. For ease of visualization, this example is restricted to two dimensions. Of course, this scenario could easily be simulated by MD but we deliberately present simple scenarios first for purposes of detail visualization. The four panels in Fig. 5.6a–d illustrate the distribution of repeatoms and sampling atoms along with the QC mesh. Automatic mesh adaptation leads to local refinement underneath the indenter and around lattice defects. The latter are visualized by plotting the centrosymmetry parameter [40] of sampling atoms (which agree with lattice sites in the fully resolved regions).

Figure 5.7 shows analogous results obtained from a pyramidal indenter penetrating into the same Cu single-crystal. As before, full atomistic resolution is restricted to those regions where it is indeed required: underneath the indenter as well as in the vicinity of lattice defects. Figure 5.7c, d shows the spreading of dislocations into the crystal after emission from the indenter, resulting in full resolution in the wake of the dislocations. The remainder of the simulation domain remains coarse-grained, thus allowing for efficient simulations having significantly fewer degrees of freedom than full atomistic calculations. As before, the distribution of repeatoms and sampling atoms is shown along with the QC mesh.

The curves of load vs. indentation depth for both cases of spherical and pyramidal indenters in two dimensions are summarized in Fig. 5.8. As can be expected from experiments, results demonstrate broad hysteresis loops stemming from incipient plasticity underneath the indenters. Data also show pronounced size effects in case of the spherical indenter as well as clear geometrical effects for the (self-similar) pyramidal indenters.

Figures 5.9 and 5.10 show 3D nanoindentation simulations with spherical and pyramidal indenters, respectively. Both graphics show results for Cu single-crystals modeled by an EAM potential [18]. The spherical indenter has a radius of 40 nm and results are shown up to an indentation depth of 3 nm; the pyramidal indenter has an angle of 65.3° against the vertical axis and a maximum indentation depth of 5 nm. Via the centrosymmetry parameter, lattice defects have been identified and highlighted (for better visibility, only those atoms are shown which contribute to lattice defects as identified by a higher centrosymmetry parameter).

As shown in these examples, the QC method efficiently reduces computational complexity by assigning full atomistic resolution where it is indeed required (underneath the indenter and near defects). While full resolution provides locally the same accuracy of molecular statics or dynamics, the QC approximation efficiently coarse-grains the remainder of the model domain, thereby allowing for simulations of significantly larger sample sizes. Similarly, by placing grain or twin boundaries as well as cavities and pre-existing defects in the crystal underneath the indenter, the QC method has been used to study defect interactions (again, the interested reader is referred to [81] for a full list of references).

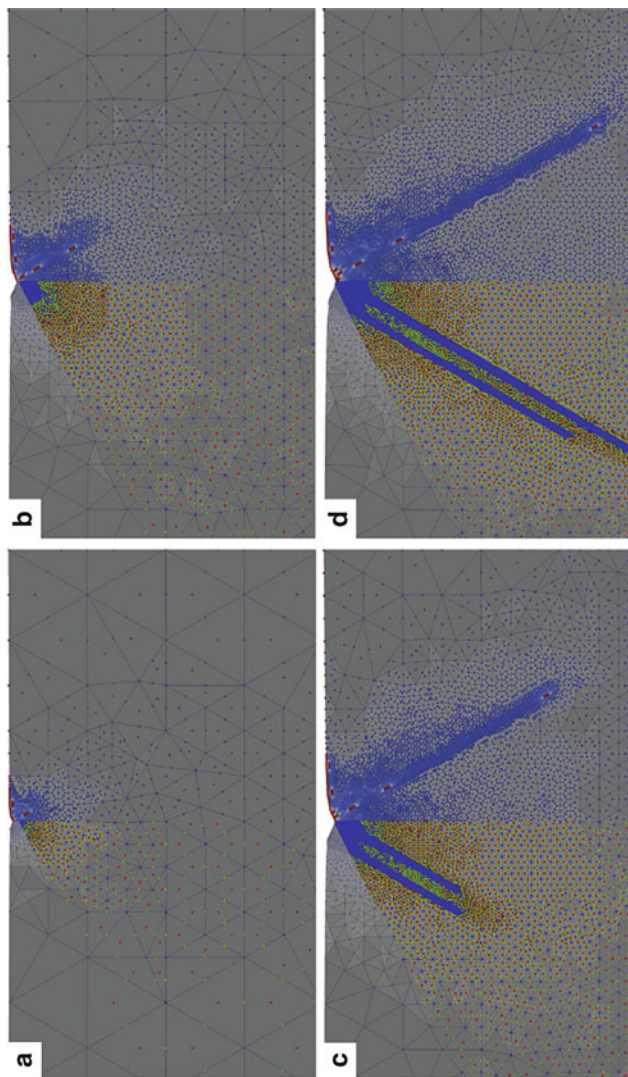


Fig. 5.7 Nanoindentation into a Cu single-crystal with a conical indenter, showing the distribution of repatoms, sampling atoms, the QC mesh, and the local centrosymmetry. Colors and panel partitioning are identical to those of Fig. 5.6a–d

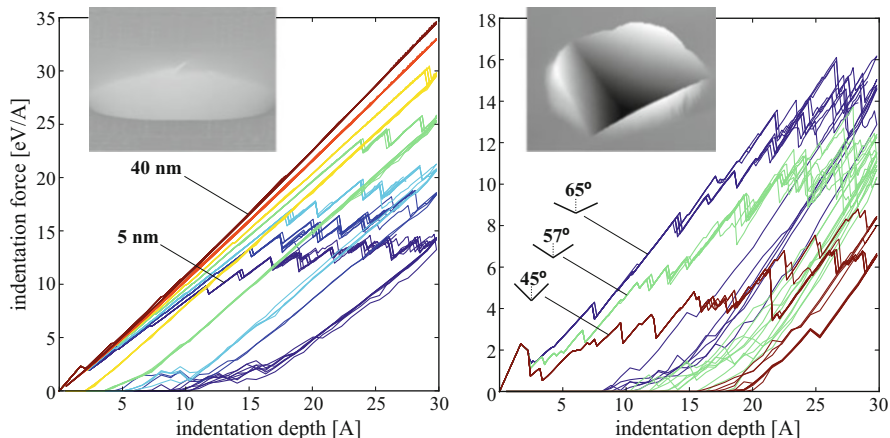


Fig. 5.8 Load vs. indentation depth for spherical indenters (of radii 5, 7.5, 10, 15, 20, 30, and 40 nm) and pyramidal indenters (of different pyramidal angles) in 2D for a (100) single-crystalline Cu, sample

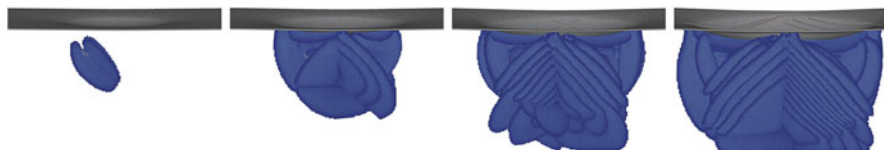


Fig. 5.9 QC Simulation of 3D nanoindentation with a spherical indenter (radius 40 nm) into single-crystalline (100) Cu up to a penetration depth of about 3 nm, for details see [5]

5.3.2 Surface Effects

Surface effects play an important role in the mechanics of nanoscale structures and devices. At those small scales, the abundance of free surfaces and the associated high surface-to-volume ratios give rise to—both elastic and plastic—size effects. Using the QC approximation near free surfaces introduces errors because (1) the associated interpolation of atomic positions may prevent surface relaxation and (2) as a consequence of the chosen summation rule, atoms below the surface may be represented by those on the surface and vice versa. The fully nonlocal QC method combined with the second-order summation rules of [5] reduces the errors near free surfaces and therefore has been utilized extensively to model deformation mechanisms near free surfaces, see, e.g., [4].

As an example, consider a thin single-crystalline plate (thickness 12 nm) with a cylindrical hole, which is being pulled uniaxially at remote locations far away from the hole. Near the hole, full atomistic resolution is required to capture defect mechanisms, but MD simulations are too expensive to model large plates. Common MD solutions focus on a small plate instead and either apply periodic boundary conditions (which introduces artifacts due to void interactions) or apply the remote

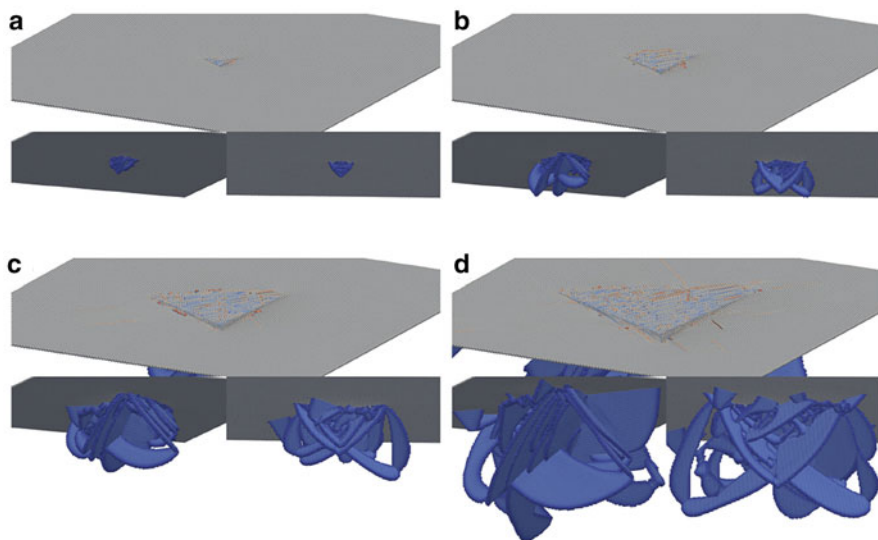


Fig. 5.10 QC simulation of 3D nanoindentation with a pyramidal indenter (angle of 65.3° against the vertical axis) into single-crystalline (100) Cu up to a penetration depth of about 5 nm

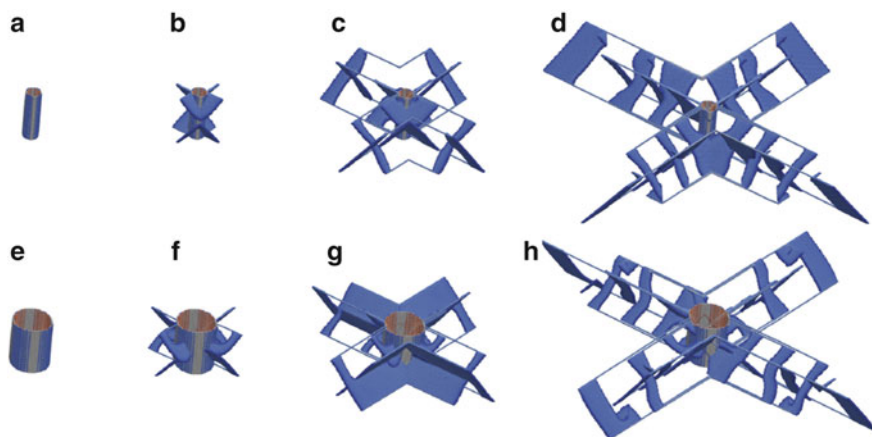


Fig. 5.11 QC simulation of dislocations emitted from cylindrical holes in thin films of single-crystalline Cu (hole radii are 1.5 and 4.5 nm in the top and bottom graphics, respectively) at strains of (a) 1.40 %, (b) 1.63 %, (c) 1.88 %, (d) 2.13 % and (e) 1.33 %, (f) 1.50 %, (g) 1.73 %, (h) 1.93 %

boundary conditions directly (which also introduces artifacts due to edge effects). Here, we use full atomistic resolution near the hole and efficiently coarsen the remaining simulation domain. By using the second-order summation rule of [4], the coarsening has no noticeable impact on the representation of the free surface. Figure 5.11 illustrates the microstructural evolution for hole radii of 1.5 and 4.5 nm.

Dislocations are emitted from the hole at a critical strain level (which increases as the hole radius decreases); the particular dislocation structures are constrained by the free surfaces at the top and bottom.

5.3.3 Truss Networks

As discussed above, the QC method applies not only to atomic lattices but can also form the basis for the coarse-graining of discrete structural lattices, as long as a thermodynamic potential is available which depends on nodal degrees of freedom. For elastic loading, the potential follows from the strain energy stored within structural components. When individual truss members are loaded beyond the elastic limit, extensions of classical QC are required in order to introduce internal variables and account for such effects as plastic flow, or truss member contact and friction. For such scenarios, effective potentials can be defined, e.g., by using the virtual power theorem [7, 9, 10]. Alternatively, variational constitutive updates [60] can be exploited to introduce effective incremental potentials, as will be shown here for a truss network. For simplicity, we restrict our study to elastic-plastic bars which undergo only nonlinear stretching deformation and large rotations (but do not deform in bending).

Let us briefly review the constitutive model for elastic-plastic trusses used in the following example. Consider a truss structure consisting of two-node bars having undeformed lengths L_{ij} and deformed lengths $r_{ij} = |\mathbf{r}_{ij}| = |\mathbf{q}_i - \mathbf{q}_j|$ with nodal positions \mathbf{q}_i ($i = 1, \dots, N$). The total strain of each bar is given by $\varepsilon = (r_{ij} - L_{ij})/L_{ij}$. By using variational constitutive updates [60], we can introduce an effective potential for elastic-plastic bars. To this end, we choose as history variables ε_p^n (the plastic strain) and e_p^n (the accumulated plastic strain) for each bar, and we update these history variables at each converged load step n as in classical computational plasticity. In linearized strains, the elastic response of each bar is characterized by $\sigma = E(\varepsilon - \varepsilon_p)$ with axial stress σ and Young's modulus E . Further, assume that the full elastic-plastic stress-strain response is piecewise linear; i.e., under monotonic loading, the bar will first yield at a stress τ_0 followed by linear hardening with a slope of $2EH/(E + 2H)$ with some hardening modulus H . Thus, for monotonic loading, we assume

$$\sigma = \begin{cases} E\varepsilon, & \text{if } \varepsilon \leq \tau_0/E, \\ \tau_0 + 2H/(E + 2H)(E\varepsilon - \tau_0), & \text{if } \varepsilon > \tau_0/E, \end{cases} \quad (5.21)$$

and the analysis for non-monotonic loading can be carried out analogously. This model can be cast into an effective potential using variational constitutive updates as follows.

Let us discretize the time response into time steps Δt and define the stress and strain at time $t^n = n \cdot \Delta t$ as σ^n and ε^n (the internal variables follow analogously).

After each load increment, we must determine the new internal variables

$$\varepsilon_p^{n+1} = \varepsilon_p^n + \Delta\varepsilon_p, \quad e_p^{n+1} = e_p^n + |\Delta\varepsilon_p|. \quad (5.22)$$

Assume an elastic-plastic effective energy density is given by

$$W(\varepsilon^{n+1}, \Delta\varepsilon_p; \varepsilon_p^n, e_p^n) = \frac{E}{2} [\varepsilon^{n+1} - (\varepsilon_p^n + \Delta\varepsilon_p)]^2 + H (e_p^n + |\Delta\varepsilon_p|)^2 + \Delta t \tau_0 \left| \frac{\Delta\varepsilon_p}{\Delta t} \right|, \quad (5.23)$$

where the first term represents the elastic energy at the new load step $n + 1$, the second term represents linear plastic hardening with hardening modulus H , and the final term defines dissipation in a rate-independent manner (τ_0 is again the yield stress, and $\Delta t = t_{n+1} - t_n > 0$ is taken as a constant time increment). The potential energy of a bar with cross-section A and length L_{ij} is now the above energy density multiplied by the bar volume AL_{ij} . Using the theory of [60], an effective potential energy of the bar can be defined as

$$V(\mathbf{q}_i^{n+1}, \mathbf{q}_j^{n+1}; \varepsilon_p^n, e_p^n) = AL_{ij} \cdot \inf_{\Delta\varepsilon_p} \left\{ W \left(\frac{r_{ij}^{n+1} - L_{ij}}{L_{ij}}, \Delta\varepsilon_p; \varepsilon_p^n, e_p^n \right) \right\}. \quad (5.24)$$

One can easily show that this potential recovers the above elastic-plastic bar model as follows. Minimization can be carried out analytically for this simple case. In particular, the stationarity condition yields the kinetic rule of plastic flow:

$$\frac{\partial W}{\partial \Delta\varepsilon_p} = -E (\varepsilon^{n+1} - \varepsilon_p^n - \Delta\varepsilon_p) + 2H (e_p^n + |\Delta\varepsilon_p|) + \tau_0 \operatorname{sign} \Delta\varepsilon_p = 0. \quad (5.25)$$

Consider first the case of $\Delta\varepsilon_p > 0$, which leads to

$$\Delta\varepsilon_p = \frac{E (\varepsilon^{n+1} - \varepsilon_p^n) - (\tau_0 + 2He_p^n)}{E + 2H} > 0. \quad (5.26)$$

Analogously, for $\Delta\varepsilon_p < 0$ we have

$$\Delta\varepsilon_p = \frac{E (\varepsilon^{n+1} - \varepsilon_p^n) + (\tau_0 + 2He_p^n)}{E + 2H} < 0. \quad (5.27)$$

If none of the two inequalities is satisfied, the bar deforms elastically and $\Delta\varepsilon_p = 0$. The stress in the bar connecting nodes i and j at the new step t^n is thus given by

$$\sigma_{ij}^{n+1} = E (\varepsilon^n - [\varepsilon_{p,ij}^n + \Delta\varepsilon_{p,ij}]), \quad (5.28)$$

and the corresponding axial bar force is $f_{ij} = A\sigma_{ij}$. Note that for monotonic loading this recovers (5.21). In other words, the above elastic-plastic model can be cast

into the effective potential (5.24). Finally, a failure criterion can be included by defining a critical stress σ_{cr} or ε_{cr} and removing bars whose stress or strain reaches the maximum allowable value.

The total Hamiltonian of the truss structure with nodal positions $\mathbf{q} = \{\mathbf{q}_1, \dots, \mathbf{q}_N\}$ and momenta $\mathbf{p} = \{\mathbf{p}_1, \dots, \mathbf{p}_N\}$ becomes

$$\mathcal{H}(\mathbf{q}, \mathbf{p}) = \sum_{i=1}^N \frac{|\mathbf{p}_i|^2}{2m_i} + \sum_{i=1}^N \sum_{j \in \mathcal{C}(i)} V(\mathbf{q}_i^{n+1}, \mathbf{q}_j^{n+1}; \varepsilon_{p,ij}^n, e_{p,ij}^n), \quad (5.29)$$

where we assumed that the mass of each bar is lumped to its nodes, so m_i represents the total mass of node i . $\mathcal{C}(i)$ denotes the star of each node, i.e. the set of all adjacent nodes connected to node i through a bar. As the structure of (5.29) is identical to that of atomistics, cf. (5.1), the QC method can be applied in the very same manner as described above for atomistic ensembles, including summation/sampling rules as well as adaptive remeshing. We note that the sums in (5.29) only involve nearest-neighbor interactions, which is why no force artifacts are expected from node-based summation rules as well as from those of [5], even in non-uniform meshes (as long as elements are sufficiently large).

As an example of this approach, we show simulation results for a three-point bending test of a periodic truss lattice with an initial notch. For small numbers of truss members, such simulations can efficiently be run with full resolution (i.e., modeling each truss member as a bar element). Advances in additive manufacturing over the past decade have continuously pushed the frontiers of fabricating micron- and nanometer-sized truss structures. This has resulted in periodic and hierarchical truss lattices with an unprecedented architectural design space of (meta)material properties. As a consequence, modeling techniques are required that can efficiently predict deformation and failure mechanisms in truss structures containing millions or billions of individual truss members. The 3D three-point bending scenario of Fig. 5.12 is one such example, where the QC method reduces computational complexity by efficient coarse-graining of the bar network (bars are assumed to be monolithic and slender, undergoing the stretching-dominated elastic-plastic model described above with a failure strain of 10 %). Loads are applied by three cylindrical indenter potentials. To account for manufacturing imperfections and to induce local failure, we vary the elastic modulus of all truss members by a Gaussian distribution (with a standard deviation of 50 % of the nominal truss stiffness). Figure 5.12 compares the simulated truss deformation and stress distribution before and after crack propagation. (a) and (b) demonstrate schematically the coarse-grained nodes, whereas (c) through (f) illustrate the advancing crack front in the fully resolved region. Like in the atomistic examples in the previous sections, the QC method allows us to efficiently model large periodic systems with locally full resolution where needed.

Of course, this is only an instructive example. Truss members may be subject to flexural deformation, nodes may contribute to deformation mechanisms, and during truss compression one commonly observes buckling and densification accompanied

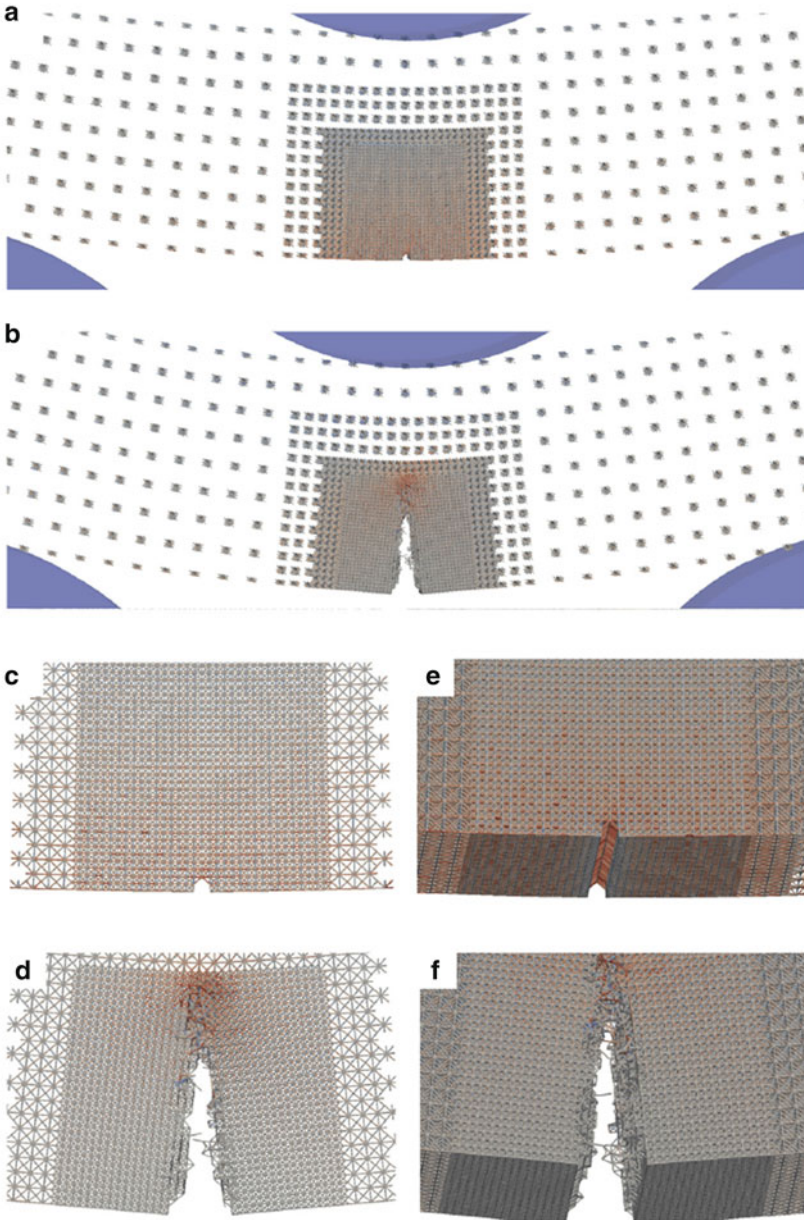


Fig. 5.12 Failure of a periodic 3D truss network under three-point bending; color-code indicates stresses within truss members (in order to account for imperfections and stress concentrations; stresses scaled to maximum). (a) and (b) visualize the representative nodes in the coarse-grained QC description (full resolution around the notch and coarsening away from the notch; the three indenters are shown as *blue balls*). (c/e) and (d/f) show, respectively, the deformed structure with its stress distribution before and after the crack has advanced

by truss member contact and friction. Model extensions for such effects have been proposed recently and are subject to ongoing research, see, e.g., [7, 9, 10].

5.4 Summary and Open Challenges

We have reviewed the fundamental concepts as well as a variety of extensions of the traditional quasicontinuum (QC) method for concurrent scale-coupling simulations with a focus on coarse-grained atomistics. This technique is solely based on interatomic potentials without the need for further empirical or phenomenological constitutive relations. Coarse-graining is achieved through the selection of representative atoms (and the interpolation of atomic positions from the set of repatoms), the introduction of sampling or summation rules (to approximate thermodynamic quantities based on a small set of sampling atoms and associated weights), and model adaptation schemes (to restrict full atomistic resolution to those regions where it is indeed beneficial). For each of those three QC pillars, a multitude of variations have been proposed and implemented. Important extensions of the method include multilattices, finite temperature, mass and heat transfer, long-range and dissipative interactions, to name but a few of those discussed in this chapter. It is important to note that the focus here has been on the QC method as a computational tool to facilitate scale-bridging simulations; as such, we have emphasized modeling concepts and applications rather than the mathematical proofs of convergence or stability (the interested reader is referred to the rich literature in this field of research, see, e.g., [29] and the references therein as well as the website [81]). Among all existing QC flavors, we have chosen a fully nonlocal QC formulation for our simulation examples to demonstrate its application to crystal plasticity and periodic truss networks.

Although the QC method was established almost two decades ago, many challenges have remained and new ones have aroused. These include, among others:

- *Adaptive coarsening*: adaptive model refinement may be geometrically challenging in practice but it is conceptually sound, ultimately turning all lattice sites into repatoms and sampling atoms and thus recovering (locally) molecular dynamics or statics. Model coarsening, by contrast, is challenging conceptually and a key open problem in many QC research codes due to the Lagrangian formulation. Overcoming this difficulty will allow to efficiently coarsen the model by removing full resolution (e.g., in the wake of a traveling lattice

defect which leaves behind a perfect crystal that is now fully resolved). Without adaptive model coarsening, simulations will accumulate atomistic resolution and ultimately turn large portions of the model domain into full MD, thus producing prohibitive computational expenses.

- *Large-scale simulations*: the number of existing massively parallel, distributed-memory QC implementations is small for a variety of reasons, especially in three dimensions. This limits the size of domains that can be simulated.
- *Dynamics* is a perpetual problem of the QC method. Non-uniform meshes result in wave reflections and wave refraction, which affects phonon motion and thereby corrupts heat propagation within the solid. For these reasons, dynamic QC simulations call for new approaches. Several finite-temperature QC formulations have aimed at overcoming some of the associated problems, but those generally come with phenomenological or simplifying assumptions.
- *Mass and heat transfer* is intimately tied to the long-term dynamics of a (coarse-grained) atomistic ensemble. Recent progress [88] has enabled the computational treatment via statistical mechanics combined with mean-field theory, yet such approaches require constitutive relations for heat and mass transfer at the atomic scale or effective transport equations, and they have not been explored widely.
- *Potentials*: every atomistic simulation stands and falls by the accuracy and reliability of its interatomic potentials. Unlike MD, QC may require conceptual extensions when it comes to, e.g., long-range interactions or interaction potentials that not only depend on the positions of the atomic nuclei.
- *Surfaces* play a crucial role in small-scale structures and devices and most QC variants do not properly account for free surfaces (misrepresenting or not at all accounting for surface relaxation). Improved surface representations are hence an open area of research, see, e.g., [4] for a recent discussion.
- *Structures*: rather recently, the QC approximation has been applied to truss and fiber networks where new challenges arise due to the complex interaction mechanisms (including, e.g., plasticity, failure, or contact). This branch of the QC family is still in its early stages with many promising applications.
- *Imperfections*: The QC method assumes perfect periodicity of the underlying (crystal or truss) lattice. When geometric imperfections play a dominant role (such as in many nano- and microscale truss networks), new extensions may be required to account for random or systematic variations within the arrangement of representative nodes, all the way to non-periodic or irregular systems.

Of course, this can only serve as a short excerpt of the long list of open challenges associated with the family of QC methods and as an open playground for those interested in scale-bridging simulations.

Acknowledgements The authors gratefully acknowledge support from the National Science Foundation (NSF) under grant number CMMI-123436.

References

1. A. Abdulle, P. Lin, A.V. Shapeev, Numerical methods for multilattices. *Multiscale Model. Simul.* **10**(3), 696–726 (2012)
2. F.F. Abraham, J.Q. Broughton, N. Bernstein, E. Kaxiras, Spanning the continuum to quantum length scales in a dynamic simulation of brittle fracture. *Europhys. Lett.* **44**(6), 783 (1998)
3. J.S. Amelang, D.M. Kochmann, Surface effects in nanoscale structures investigated by a fully-nonlocal energy-based quasicontinuum method, *Mechanics of Materials* **90**, 166–184 (2015)
4. J.S. Amelang, G.N. Venturini, D.M. Kochmann, Summation rules for a fully-nonlocal energy-based quasicontinuum method, *J. Mech. Phys. Solids* **82**, 378–413 (2015)
5. J.S. Amelang, A fully-nonlocal energy-based formulation and high-performance realization of 842 the quasicontinuum method. PhD thesis, California Institute of Technology (2015)
6. M. Ariza, I. Romero, M. Ponga, M. Ortiz, Hotqc simulation of nanovoid growth under tension in copper. *Int. J. Fract.* **174**, 75–85 (2012)
7. L.A.A. Beex, R.H.J. Peerlings, M.G.D. Geers, A quasicontinuum methodology for multiscale analyses of discrete microstructural models. *Int. J. Numer. Methods Eng.* **87**(7), 701–718 (2011)
8. L.A.A. Beex, C.W. Verberne, R.H.J. Peerlings, Experimental identification of a lattice model for woven fabrics: application to electronic textile. *Compos. Part A Appl Sci. Manuf.* **48**, 82–92 (2013)
9. L.A.A. Beex, R.H.J. Peerlings, M.G.D. Geers, A multiscale quasicontinuum method for dissipative lattice models and discrete networks. *J. Mech. Phys. Solids* **64**, 154–169 (2014)
10. L.A.A. Beex, R.H.J. Peerlings, M.G.D. Geers, A multiscale quasicontinuum method for lattice models with bond failure and fiber sliding. *Comput. Methods Appl. Mech. Eng.* **269**, 108–122 (2014)
11. L.A.A. Beex, R.H.J. Peerlings, M.G.D. Geers, Central summation in the quasicontinuum method. *J. Mech. Phys. Solids* **70**, 242–261 (2014)
12. T. Belytschko, S.P. Xiao, Coupling methods for continuum model with molecular model. *Int. J. Multiscale Comput. Eng.* **1**(1), 115–126 (2003)
13. S. Brinckmann, D.K. Mahajan, A. Hartmaier, A scheme to combine molecular dynamics and dislocation dynamics. *Model. Simul. Mater. Sci. Eng.* **20**(4), 045001 (2012)
14. J.Q. Broughton, F.F. Abraham, N. Bernstein, E. Kaxiras, Concurrent coupling of length scales: methodology and application. *Phys. Rev. B* **60**, 2391–2403 (1999)
15. P.W. Chung, Computational method for atomistic homogenization of nanopatterned point defect structures. *Int. J. Numer. Methods Eng.* **60**(4), 833–859 (2004)
16. J.D. Clayton, P.W. Chung, An atomistic-to-continuum framework for nonlinear crystal mechanics based on asymptotic homogenization. *J. Mech. Phys. Solids* **54**(8), 1604–1639 (2006)
17. W.A. Curtin, R.E. Miller, Atomistic/continuum coupling in computational materials science. *Model. Simul. Mater. Sci. Eng.* **11**(3), R33 (2003)
18. X.D. Dai, Y. Kong, J.H. Li, B.X. Liu, Extended finnis-sinclair potential for bcc and fcc metals and alloys. *J. Phys. Condens. Matter* **18**, 4527–4542 (2006)
19. M.S. Daw, M.I. Baskes, Embedded-atom method: derivation and application to impurities, surfaces, and other defects in metals. *Phys. Rev. B* **29**, 6443–6453 (1984)
20. K. Dayal, J. Marshall, A multiscale atomistic-to-continuum method for charged defects in electronic materials, in *Presented as the Society of Engineering Science 2011 Annual Technical Conference*, Evanston (2011)
21. D.J. Diestler, Z.B. Wu, X.C. Zeng, An extension of the quasicontinuum treatment of multiscale solid systems to nonzero temperature. *J. Chem. Phys.* **121**, 9279–9282 (2004)
22. M. Dobson, R.S. Elliott, M. Luskin, E.B. Tadmor, A multilattice quasicontinuum for phase transforming materials: cascading cauchy born kinematics. *J. Comput. Aided Mater. Des.* **14**, 219–237 (2007)

23. M. Dobson, R.S. Elliott, M. Luskin, E.B. Tadmor, A multilattice quasicontinuum for phase transforming materials: cascading cauchy born kinematics. *J. Comput. Aided Mater. Des.* **14**(1), 219–237 (2007)
24. M. Dobson, M. Luskin, C. Ortner, Accuracy of quasicontinuum approximations near instabilities. *J. Mech. Phys. Solids* **58**, 1741–1757 (2010)
25. M. Dobson, M. Luskin, C. Ortner, Sharp stability estimates for the force-based quasicontinuum approximation of homogeneous tensile deformation. *Multiscale Model. Simul.* **8**, 782–802 (2010)
26. M. Dobson, M. Luskin, C. Ortner, Stability, instability, and error of the force-based quasicontinuum approximation. *Arch. Ration. Mech. Anal.* **197**, 179–202 (2010)
27. L.M. Dupuy, E.B. Tadmor, R.E. Miller, R. Phillips, Finite-temperature quasicontinuum: molecular dynamics without all the atoms. *Phys. Rev. Lett.* **95**, 060202 (2005)
28. B. Eidel, A. Stukowski, A variational formulation of the quasicontinuum method based on energy sampling in clusters. *J. Mech. Phys. Solids* **57**, 87–108 (2009)
29. M.I. Espanol, D.M. Kochmann, S. Conti, M. Ortiz, A gamma-convergence analysis of the quasicontinuum method. *SIAM Multiscale Model. Simul.* **11**, 766–794 (2013)
30. F. Feyel, J.-L. Chaboche, Fe₂ multiscale approach for modelling the elastoviscoplastic behaviour of long fibre sic/ti composite materials. *Comput. Methods Appl. Mech. Eng.* **183**(3–4), 309–330 (2000)
31. S.M. Foiles, M.I. Baskes, M.S. Daw, Embedded-atom-method functions for the fcc metals Cu, Ag, Au, Ni, Pd, Pt, and their alloys. *Phys. Rev. B* **33**, 7983–7991 (1986)
32. V. Gavini, K. Bhattacharya, M. Ortiz, Quasi-continuum orbital-free density-functional theory: a route to multi-million atom non-periodic DFT calculation. *J. Mech. Phys. Solids* **55**(4), 697–718 (2007)
33. M. Gunzburger, Y. Zhang, A quadrature-rule type approximation to the quasi-continuum method. *Multiscale Model. Simul.* **8**(2), 571–590 (2010)
34. S. Hai, E.B. Tadmor, Deformation twinning at aluminum crack tips. *Acta Mater.* **51**, 117–131 (2003)
35. K. Hardikar, V. Shenoy, R. Phillips, Reconciliation of atomic-level and continuum notions concerning the interaction of dislocations and obstacles. *J. Mech. Phys. Solids* **49**(9), 1951–1967 (2001)
36. L. Huai-Bao, L. Jun-Wan, N. Yu-Shan, M. Ji-Fa, W. Hong-Sheng, Multiscale analysis of defect initiation on the atomistic crack tip in body-centered-cubic metal Ta. *Acta Phys. Sin.* **60**(10), 106101 (2011)
37. M. Iyer, V. Gavini, A field theoretical approach to the quasi-continuum method. *J. Mech. Phys. Sol.* **59**(8), 1506–1535 (2011)
38. S. Izvekov, G.A. Voth, A multiscale coarse-graining method for biomolecular systems. *J. Phys. Chem. B* **109**(7), 2469–2473 (2005)
39. R.A. Johnson, Alloy models with the embedded-atom method. *Phys. Rev. B* **39**, 12554–12559 (1989)
40. C.L. Kelchner, S.J. Plimpton, J.C. Hamilton, Dislocation nucleation and defect structure during surface indentation. *Phys. Rev. B* **58**, 11085–11088 (1998)
41. W.K. Kim, M. Luskin, D. Perez, A.F. Voter, E.B. Tadmor, Hyper-qc: an accelerated finite-temperature quasicontinuum method using hyperdynamics. *J. Mech. Phys. Solids* **63**, 94–112 (2014)
42. J. Knap, M. Ortiz, An analysis of the quasicontinuum method. *J. Mech. Phys. Solids* **49**(9), 1899–1923 (2001)
43. D.M. Kochmann, G.N. Venturini, A meshless quasicontinuum method based on local maximum-entropy interpolation. *Model. Simul. Mater. Sci. Eng.* **22**, 034007 (2014)
44. Y. Kulkarni, Coarse-graining of atomistic description at finite temperature. PhD thesis, California Institute of Technology (2007)
45. Y. Kulkarni, J. Knap, M. Ortiz, A variational approach to coarse graining of equilibrium and non-equilibrium atomistic description at finite temperature. *J. Mech. Phys. Solids* **56**, 1417–1449 (2008)

46. S. Kwon, Y. Lee, J.Y. Park, D. Sohn, J.H. Lim, S. Im, An efficient three-dimensional adaptive quasicontinuum method using variable-node elements. *J. Comput. Phys.* **228**(13), 4789–4810 (2009)
47. J. Li, J. Mei, Y. Ni, H. Lu, W. Jiang, Two-dimensional quasicontinuum analysis of the strengthening and weakening effect of cu/ag interface on nanoindentation. *J. Appl. Phys.* **108**(5), 054309 (2010)
48. J. Li, H. Lu, Y. Ni, J. Mei, Quasicontinuum study the influence of misfit dislocation interactions on nanoindentation. *Comput. Mater. Sci.* **50**(11), 3162–3170 (2011)
49. X.H. Li, M. Luskin, C. Ortner, A.V. Shapeev, Theory-based benchmarking of the blended force-based quasicontinuum method. *Comput. Methods Appl. Mech. Eng.* **268**, 763–781 (2014)
50. W.K. Liu, H.S. Park, D. Qian, E.G. Karpov, H. Kadowaki, G.J. Wagner, Bridging scale methods for nanomechanics and materials. *Comput. Methods Appl. Mech. Eng.* **195**(13–16), 1407–1421 (2006)
51. H. Lu, Y. Ni, J. Mei, J. Li, H. Wang, Anisotropic plastic deformation beneath surface step during nanoindentation of fcc al by multiscale analysis. *Comput. Mater. Sci.* **58**, 192–200 (2012)
52. M. Luskin, C. Ortner, An analysis of node-based cluster summation rules in the quasicontinuum method. *SIAM J. Numer. Anal.* **47**(4), 3070–3086 (2009)
53. M. Luskin, C. Ortner, B. Van Koten, Formulation and optimization of the energy-based blended quasicontinuum method. *Comput. Methods Appl. Mech. Eng.* **253**, 160–168 (2013)
54. J. Marian, G. Venturini, B.L. Hansen, J. Knap, M. Ortiz, G.H. Campbell, Finite-temperature extension of the quasicontinuum method using langevin dynamics: entropy losses and analysis of errors. *Model. Simul. Mater. Sci. Eng.* **18**(1), 015003 (2010)
55. J. Marshall, K. Dayal, Atomistic-to-continuum multiscale modeling with long-range electrostatic interactions in ionic solids. *J. Mech. Phys. Solids* **62**, 137–162 (2014). Sixtieth anniversary issue in honor of Professor Rodney Hill
56. C. Miehe, J. Schröder, J. Schotte, Computational homogenization analysis in finite plasticity simulation of texture development in polycrystalline materials. *Comput. Methods Appl. Mech. Eng.* **171**, 387–418 (1999)
57. R.E. Miller, E.B. Tadmor, A unified framework and performance benchmark of fourteen multiscale atomistic/continuum coupling methods. *Model. Simul. Mater. Sci. Eng.* **17**, 053001 (2009)
58. R.E. Miller, M. Ortiz, R. Phillips, V. Shenoy, E.B. Tadmor, Quasicontinuum models of fracture and plasticity. *Eng. Fract. Mech.* **61**, 427–444 (1998)
59. A.K. Nair, D.H. Warner, R.G. Hennig, W.A. Curtin, Coupling quantum and continuum scales to predict crack tip dislocation nucleation. *Scr. Mater.* **63**(12), 1212–1215 (2010)
60. M. Ortiz, L. Stainier, The variational formulation of viscoplastic constitutive updates. *Comput. Methods Appl. Mech. Eng.* **171**(3–4), 419–444 (1999)
61. C. Ortner, A priori and a posteriori analysis of the quasinonlocal quasicontinuum method in 1d. *Math. Comput.* **80**(275), 1265–1285 (2011)
62. H.S. Park, E.G. Karpov, W.K. Liu, P.A. Klein, The bridging scale for two-dimensional atomistic/continuum coupling. *Philos. Mag.* **85**(1), 79–113 (2005)
63. J.Y. Park, S. Im, Adaptive nonlocal quasicontinuum for deformations of curved crystalline structures. *Phys. Rev. B* **77**, 184109 (2008)
64. J.Y. Park, C.-H. Park, J.-S. Park, K.-J. Kong, H. Chang, S. Im, Multiscale computations for carbon nanotubes based on a hybrid qm/qc (quantum mechanical and quasicontinuum) approach. *J. Mech. Phys. Solids* **58**(2), 86–102 (2010)
65. R. Phillips, D. Rodney, V. Shenoy, E. Tadmor, M. Ortiz, Hierarchical models of plasticity: dislocation nucleation and interaction. *Model. Simul. Mater. Sci. Eng.* **7**, 769–780 (1999)
66. M. Ponga, M. Ortiz, M.P. Ariza, Finite-temperature non-equilibrium quasi-continuum analysis of nanovoid growth in copper at low and high strain rates. *Mech. Mater.* **90**, 253–267 (2015)
67. A. Ramasubramaniam, M. Itakura, E.A. Carter, Interatomic potentials for hydrogen in α -iron based on density functional theory. *Phys. Rev. B* **79**, 174101 (2009)

68. I. Ringdalen Vatne, E. Ostby, C. Thaulow, Multiscale simulations of mixed-mode fracture in bcc-fe. *Model. Simul. Mater. Sci. Eng.* **19**(8), 085006 (2011)
69. R.E. Rudd, J.Q. Broughton, Coarse-grained molecular dynamics: nonlinear finite elements and finite temperature. *Phys. Rev. B* **72**, 144104 (2005)
70. J. Schröder, Homogenisierungsmethoden der nichtlinearen Kontinuumsmechanik unter Beachtung von Stabilitätsproblemen. Habilitation thesis, Universität Stuttgart (2000)
71. V.B. Shenoy, R. Miller, E.B. Tadmor, R. Phillips, M. Ortiz, Quasicontinuum models of interfacial structure and deformation. *Phys. Rev. Lett.* **80**, 742–745 (1998)
72. V.B. Shenoy, V. Shenoy, R. Phillips, Finite temperature quasicontinuum methods. *Mater. Res. Soc. Symp. Proc.* **538**, 465–471 (1999)
73. M.S. Shephard, C. Picu, D.K. Datta, Composite grid atomistic continuum method: an adaptive approach to bridge continuum with atomistic analysis. *Int. J. Multiscale Comput. Eng.* **2**(3) (2004)
74. L.E. Shilkrot, R.E. Miller, W.A. Curtin, Multiscale plasticity modeling: coupled atomistics and discrete dislocation mechanics. *J. Mech. Phys. Solids* **52**, 755–787 (2004)
75. T. Shimokawa, J.J. Mortensen, J. Schiøtz, K.W. Jacobsen, Matching conditions in the quasicontinuum method: removal of the error introduced at the interface between the coarse-grained and fully atomistic region. *Phys. Rev. B* **69**, 214104 (2004)
76. T. Shimokawa, T. Kinari, S. Shintaku, Interaction mechanism between edge dislocations and asymmetrical tilt grain boundaries investigated via quasicontinuum simulations. *Phys. Rev. B* **75**, 144108 (2007)
77. V. Sorkin, R.S. Elliott, E.B. Tadmor, A local quasicontinuum method for 3d multilattice crystalline materials: application to shape-memory alloys. *Model. Simul. Mater. Sci. Eng.* **22**(5), 055001 (2014)
78. P. Suryanarayana, Coarse-graining Kohn-Sham density functional theory. PhD thesis, California Institute of Technology (2011)
79. P. Suryanarayana, K. Bhattacharya, M. Ortiz, Coarse-graining Kohn-Sham Density Functional Theory. *J. Mech. Phys. Solids* **61**(1), 38–60 (2013)
80. E.B. Tadmor, S. Hai, A Peierls criterion for the onset of deformation twinning at a crack tip. *J. Mech. Phys. Solids* **51**(5), 765–793 (2003)
81. E.B. Tadmor, R.E. Miller, <http://qcmethod.org/> (2016)
82. E.B. Tadmor, M. Ortiz, R. Phillips, Quasicontinuum analysis of defects in solids. *Philos. Mag. A* **73**(6), 1529–1563 (1996)
83. E.B. Tadmor, R. Miller, R. Philipps, M. Ortiz, Nanoindentation and incipient plasticity. *J. Mater. Res.* **14**, 2233–2250 (1999)
84. E.B. Tadmor, U.V. Waghmare, G.S. Smith, E. Kaxiras, Polarization switching in PbTiO₃: an ab initio finite element simulation. *Acta Mater.* **50**(11), 2989–3002 (2002)
85. E.B. Tadmor, F. Legoll, W. Kim, L. Dupuy, R. Miller, Finite-temperature quasi-continuum. *Appl. Mech. Rev.* **65**(1), 010803 (2013)
86. Z. Tang, H. Zhao, G. Li, N.R. Aluru, Finite-temperature quasicontinuum method for multiscale analysis of silicon nanostructures. *Phys. Rev. B* **74**, 064110 (2006)
87. G.N. Venturini, Topics in multiscale modeling of metals and metallic alloys. PhD thesis, California Institute of Technology (2011)
88. G.N. Venturini, K. Wang, I. Romero, M.P. Ariza, M. Ortiz, Atomistic long-term simulation of heat and mass transport. *J. Mech. Phys. Solids* **73**, 242–268 (2014)
89. A.F. Voter, A method for accelerating the molecular dynamics simulation of infrequent events. *J. Chem. Phys.* **106**(11), 4665–4677 (1997)
90. A.F. Voter, F. Montalenti, T.C. Germann, Extending the time scale in atomistic simulation of materials. *Annu. Rev. Mater. Res.* **32**(1), 321–346 (2002)
91. K.G. Wang, M. Ortiz, M.P. Ariza, Long-term atomistic simulation of hydrogen diffusion in metals. *Int. J. Hydrog. Energy* **40**(15), 5353–5358 (2015)
92. X. Wang, X. Guo, Quasi-continuum model for the finite deformation of single-layer graphene sheets based on the temperature-related higher order cauchy-born rule. *J. Comput. Theor. Nanosci.* **10**(1), 154–164 (2013)

93. L. Ward, A. Agrawal, K.M. Flores, W. Windl, Rapid production of accurate embedded-atom method potentials for metal alloys. ArXiv e-prints (2012)
94. S. Xiao, W. Yang, A temperature-related homogenization technique and its implementation in the meshfree particle method for nanoscale simulations. *Int. J. Numer. Methods Eng.* **69**(10), 2099–2125 (2007)
95. Q. Yang, E. Biyikli, A.C. To, Multiresolution molecular mechanics: statics. *Comput. Methods Appl. Mech. Eng.* **258**, 26–38 (2013)
96. W. Yang, S. Xiao, The applications of meshfree particle methods at the nanoscale, in *Computational Science – ICCS 2005*, ed. by V.S. Sunderam, G.D. Albada, P.M.A. Sloot, J. Dongarra. Lecture Notes in Computer Science, vol. 3516 (Springer, Berlin/Heidelberg, 2005), pp. 284–291
97. H. Yoshihiko, Y. Nobuhiro, S.V. Dmitriev, K. Masanori, T. Shingo, Large scale atomistic simulation of cu/al₂o₃ interface via quasicontinuum analysis. *J. Jpn. Inst. Metals* **69**(1), 90–95 (2005)
98. W. Yu, S. Shen, Initial dislocation topologies of nanoindentation into copper film with a nanocavity. *Eng. Fract. Mech.* **77**(16), 3329–3340 (2010)